# Progress in hexagonal boron nitride (h-BN) based solid state neutron detector

*Samiul Hasan, Iftikhar Ahmad*

*Department of Electrical Engineering, University of South Carolina, Columbia, SC 29208, USA*

Corresponding author at: University of South Carolina, Columbia, SC 29208, USA.
E-mail address: shasan@email.sc.edu, ahmad@cec.sc.du

## Abstract:

This article will briefly review the progress of h-BN based solid-state metal semiconductor metal (MSM) neutron detectors. In the last decade, several groups have been working on hexagonal boron nitride (h-BN) based solid-state neutron detectors. Recently, the detection efficiency of 59% has been reported. Efficient, low-cost neutron detectors made from readily available materials are essential for various applications. Neutron detectors are widely used to detect fissile materials and nuclear power plants for security applications. The most common and widely used neutron detectors are $^3$He based, which are sometimes bulky, difficult to transport, have high absorption length, need relatively high bias voltage (>1000 V), and have low Q-value (0.764 MeV). Also, $^3$He is not readily available material. Thus, there is a strong need to find an alternative detection material. $^{10}$B isotope has a high neutron absorption cross-section, and it has been tested as a coating on the semiconducting materials. Due to the two-step process, neutron capture through $^{10}$B, and then electron-hole pair generation in a typical semiconducting material, the efficiency of these devices is not up to the mark. The progress in h-BN based detectors requires a review to envision the further improvement in this technology.

**Keywords**: h-BN, neutron detector, Solid State detector, Metal Semiconductor Metal

## 1. Introduction:

Neutrons are electrically neutral and indirect ionizing radiation [1]. They are mainly generated from nuclear fission reactions but can also be the signature of the presence of particular types of radioactive materials. The penetration depth of neutrons is large due to their charge neutrality and low mass compared to other nuclear particles. When a neutron interacts with matter, three types of events can happen [1]: elastic scattering, inelastic scattering, and radiative absorption. Both high energy (~1-2 MeV) fast neutron (elastic scattering event) and low energy (~0.025eV) thermal neutron radiative absorption event) interactions are current research topics for developing neutron detectors [2]. Highly efficient neutron detectors are essential for various applications such as oil borehole logging, neutron forensics, fissile material sensing, etc. [3,4]. The thermal neutrons are usually detected indirectly using a conversion medium [5]. Neutrons absorbing isotopes with a high microscopic neutron absorption cross-section act as the conversion medium. These isotopes release ionizing radiation such as gamma rays or charged particles upon the absorption of neutrons [6]. Different isotopes are used as neutron-absorbing media like $^3$He,

$^{6}$Li, $^{10}$B, $^{113}$Cd, $^{235}$U, $^{135}$Xe, $^{199}$Hg, where their neutron absorbing cross-sections are diverse, as shown below [7].

Table 1. Neutron absorption cross section for different isotopes [7]

| Isotope | Cross section in barn (1 barn = $10^{-24}$ cm$^2$) |
|---|---|
| $^{3}$He | 5333 |
| $^{6}$Li | 941 |
| $^{10}$B | 3838 |
| $^{113}$Cd | 20600 |
| $^{235}$U | 681 |
| $^{135}$Xe | 2720000 |
| $^{199}$Hg | 2150 |

There is a tradeoff between the feasibility of using neutron-absorbing isotope and absorption cross-section. Feasible materials can be used as a coating material in the direct semiconducting material [8,9]. The isotopes having a high neutron absorption cross-section and low atomic mass to absorb thermal neutrons are preferable [10]. Currently, $^{3}$He is the most widely used material, but it has limitations like high bias voltage, high cost, and scarcity [11–17]. We observe in Table 1, the neutron absorption cross-section of $^{3}$He is ~5333 barns, which is higher than $^{10}$B (3838 barns) [8]. But the atomic density of $^{10}$B in hexagonal boron nitride (h-BN) is higher than $^{3}$He; thus, the thermal neutron absorption cross-section is much higher [18]. It has been shown in the previous works that $^{10}$B can be a prospective replacement of $^{3}$He [19]. The reaction during thermal neutron detection in $^{10}$B can be written as shown in equations (1) and (2) [20]:

$$^{10}\mathrm{B} + {}^{1}\mathrm{n} = {}^{7}\mathrm{Li}\ (1.015\ \mathrm{MeV}) + {}^{4}\alpha\ (1.77\mathrm{MeV}) \qquad (1)$$

$$^{10}\mathrm{B} + {}^{1}\mathrm{n} = {}^{7}\mathrm{Li}^{*}\ (0.84\mathrm{MeV}) + {}^{4}\alpha^{*}\ (1.47\ \mathrm{MeV}) \qquad (2)$$

$^{10}$B isotope enriched coating layer work as a neutron to alpha particle conversion medium on semiconductors (Si/GaAs) but has very low efficiency (2%-5%) due to a two-step process [21–27]. The coating material needs to be thick so that enough neutrons can be absorbed. But the problem is byproducts of the reaction mentioned above, Li and alpha ions, can travel only 2-5 µm. Thus, this process cannot generate enough corresponding electron-hole pairs in the semiconducting materials due to the incident neutrons' energy loss at the interface and the low diffusion length of Li atoms and alpha ions [28,29]. Other candidates like $B_4C$ and pyrolytic boron nitride-based detectors are still suffering design issues and low detection efficiency [30]. Other challenges include material quality, collection of charges before recombination, etc. [31]. h-BN has been researched and developed for the last 10-15 years as prospective semiconductor neutron detector material despite all these shortcomings. In semiconductor-based neutron detectors, the absorbing event creates electron-hole pair. An external bias pushes the created electron-hole pairs in the semiconductor material towards the anode and cathode, generating an electrical signal [32]. This signal passed through external circuit elements, which are characterized by a multichannel analyzer (MCA) [32]. Thus, a semiconductor material acts as a neutron detector. Generally, semiconductor materials need to have certain properties to act as radiation detectors like large bandgap, high resistivity, small electron-hole pair energy, high material quality, low dielectric constant, high radiation hardness, and high thermal conductivity [33]. Based on the criteria mentioned above, Table 2 compares existing semiconductor-based radiation detector materials with h-BN.

Table 2. Physical parameters comparison for different semiconductor materials [34–36]

| Material | Si | Ge | CdTe | $Cd_{0.5}Zn_{0.5}Te$ | 4H SiC | a-Se | h-BN |
|---|---|---|---|---|---|---|---|
| Crystal structure | Cubic | Cubic | Cubic | Cubic | Hexagonal | Amorphous | Hexagonal |
| Production method | CZ | CZ | THM | BM, THM | PVT-Bulk, CVD-epitaxy | HVTE-Thin film | MOCVD |
| Atomic number | 14 | 32 | 48,52 | 48,30,52 | 14,6 | 34 | 5,7 |
| Density | 2.33 | 5.33 | 6.2 | 5.78 | 3.21 | 6.4 | 2.18 |
| Bandgap | 1.12 | 0.67 | 1.5 | 1.6 | 3.27 | 2.24 | ~6.4 |
| Dielectric constant | 11.7 | 16.2 | 10.2 | ~11 | 9.7 | ~6 | 4.9 |
| e-h pair creation energy | 3.62 | 2.96 | 4.43 | 4.6 | 7.28 | ~50 | 18 |
| Resistivity | $10^4$ | 50 | $10^9$ | $>10^{10}$ | $>10^{12}$ | $\sim10^{13}$ | $\sim10^{13}$ |

CZ= Czochralski, THM= Travelling Heater Method, BM= Bridgman Method, PVT= Physical Vapor Transport, CVD= Chemical Vapor Deposition, HVTE= Halide Vapor Transport Epitaxy, MOCVD= Metal-Organic Chemical Vapor Deposition

Based on material properties in Table 2, h-BN can be an ideal candidate to compete with existing commercialized thermal neutron detectors. It has a large bandgap compared to other radiation detector materials, so the radiation detectors prepared with h-BN will have low thermal noise. High resistivity compared to other materials make h-BN based detectors have low leakage current [37–39]. h-BN is reported to be grown by metal-organic chemical deposition (MOCVD) systems; thus, the growth process is robust, controllable, and produces less defective material. h-BN has the highest thermal conductivity among all the materials in the table, resulting in the effective cooling of h-BN-based devices. Li *et al*. showed a comparative chart in 2011 showing the feasibility of h-BN (Table 3) as a neutron detector, and they mentioned defect-free epitaxial growth as a challenge [31].

Table 3. Neutron detector type comparison [31]

| | $^3$He | Scintillator detector | B coated detector | BN semiconductor detector |
|---|---|---|---|---|
| Particle generated by neutron | ions | photons | Ions, electrons, holes | Ions, electrons, holes |
| Active thickness | ~10 cm | ~1 mm | ~ 100 µm | ~ 100 µm |
| Key issue | Shortage of $^3$He gas | sensitivity | sensitivity | Suitable materials |
| Response speed | ~ 1 ms | ~ 1ns | ~1 ns | 1ns |

| | | | | |
|---|---|---|---|---|
| Intrinsic detection efficiency | high | Low | Low | High |
| Cost | High | Low | Low | Low |
| Portability | Poor | Medium | High | high |

The objective of this paper is to review the recent progress and challenges in the development of h-BN based metal semiconductor metal (MSM) thermal neutron detectors. In the first part of the article, we have described the h-BN structure, growth process, and fabrication. After that, we will review the results of the fabricated devices till now and their shortcomings. Our discussion will conclude with some perceived future work for commercializing these detectors.

## 2. Materials and methods:

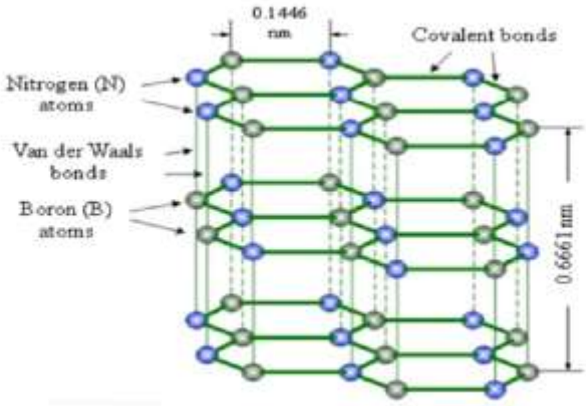

Figure 1. h-BN stacked structure [The image is reproduced from [40], with permission from SPIE]

h-BN is a group III-V semiconductor with Boron and Nitrogen atoms bonded one after another. Two $sp^2$ bonded layered configuration is very similar to hexagonal graphite. Figure 1 shows the atomic structure of h-BN, where one nitrogen atom sits next to a boron atom. Atoms in the same plane are strongly $sp^2$ bonded as a sheet, and the weak Van der Walls interaction attracts these sheets [40]. h-BN is a wide bandgap material, as mentioned in Table 1. The first principle calculation showed an interesting phenomenon reported by Jin Li *et al*. [41]. Their density functional theory-based calculations showed that bandgap is a function of symmetrical compressive strain and asymmetrical tensile strain, which can create transitions of direct bandgap to indirect bandgap property.

The experimental fabrication process for h-BN based neutron detector is illustrated in Figure 2, as mentioned in reference [32].

Figure 2. Schematic of h-BN detector fabrication process.

### 2.1 Growth of h-BN

Synthesis of h-BN can be classified into two different approaches: Top-down and Bottom-up. Figure 1 shows that h-BN has a 2D graphite-like structure with interlayer Van der Waals interactions [42,43]. These weak interactions can be easily overcome by shear forces, mechanical exfoliation, or ball milling procedures [44–48]. The problem with these top-down methods is limited yield and small flake size. The liquid exfoliation method can be considered another alternative to breaking the interlayer van der Waals forces[47,49,50]. Compared to graphene, where mechanical exfoliation is much more common, h-BN is less popular for this method as interlayer interaction is much stronger in the case of h-BN [45,47,48,51]. The top-down approaches are easy to handle compared to the bottom-up approaches, but it is hard to control the thickness, size of the flakes, and surface contamination. The bottom-up approaches can be adopted with or without a substrate. h-BN nanosheets can be grown without substrate by direct chemical reactions of precursor in the wet medium [46,52,53]. Deposition techniques like low-pressure chemical vapor deposition (CVD), catalytic CVD, plasma-enhanced CVD, and ion beam deposition are the most common bottom-up approaches [51,54–56]. CVD is a low-cost, easily controlled growth technique for III-Nitride material system specially h-BN [57,58]. There are a couple of controllable growth parameters to produce high-quality, large area, single-crystalline layered structures.

Recently, Metal-Organic Chemical Vapor Deposition (MOCVD) has been used due to less toxicity and precise control of the precursors [19,59–62]. The most important parameters that have been optimized in the case of MOCVD growth of h-BN are metal-organic precursors flow rate, growth temperature, type of carrier gas, reactor pressure, etc [41,63–69]. h-BN has a high melting temperature (~ 3000 °C), so growth requires a high temperature[70,71]. Typically, for detector applications, h-BN is grown on sapphire. First, a low temperature (~800 °C) buffer layer is grown, then the main thick detector layer is grown. The typical growth temperature for h-BN is in the range of 1300 °C to 1500 °C. Usually, the on-shelf trimthylboron (TMB)/ tryethyleboron (TEB) used as metal-organic precursor containing 20% $^{10}$B and 80% $^{11}$B. Ammonia is usually the precursor for nitrogen in the h-BN growth process. The flow rates of the precursors are precisely controlled through mass flow controllers. The growth procedure is usually done with a pulsed epitaxy sequence where the Boron and the nitrogen precursors (Triethylboron, and $NH_3$), are alternately supplied to the growth chamber to form thick films. In this process, pulse duration and their numbers are varied to get the optimized growth conditions [59], [70], [71]. The chamber pressure throughout the growth remains constant at ~10-40 torr [58], [66], [67]., X-ray diffraction methods are used to determine the crystallinity/quality of the h-BN sample [67], [72], [73]. Figure 3 shows data for a typical h-BN high-resolution X-ray diffraction scan [18]. The radial (2θ-ω) and angular (ω) scan is usually used to match the lattice parameters and calculate the defect levels from the x-ray diffraction pattern. So far, at (0 0 0 2) reflection, the minimum full-width-at-half-maxima (FWHM) of 380 arcsec has been reported [76].

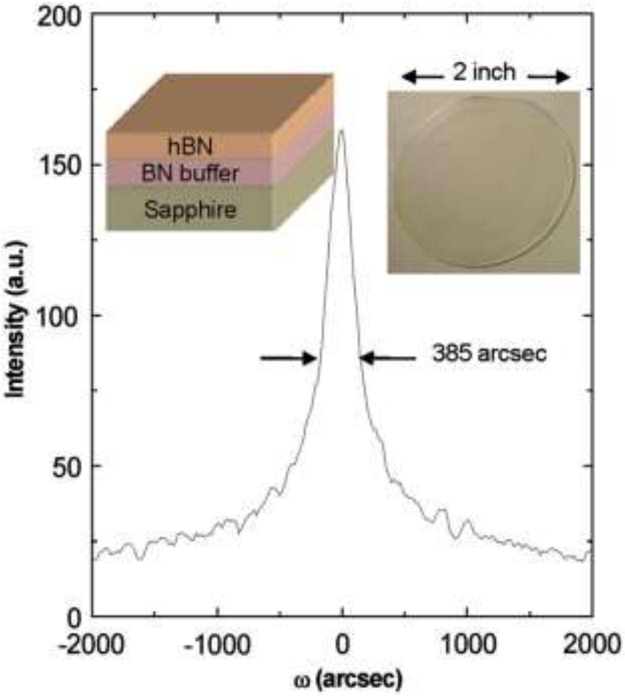

Figure 3. Angular scan to find out FWHM [The image is reproduced from [31] with permission from Elsevier]

The summary of MOCVD-based growth methods is presented in table 4.

Table 4. Growth methods for h-BN

| **Precursors** | **Substrate** | **Carrier gas** | **Growth Temp. (°C)** | **Pressure (torr)** | **Film quality** | **Ref.** |
|---|---|---|---|---|---|---|
| Triethylamine borane and ammonia (V/III ratio varied between 450 and 2700) | c-plane sapphire (varying surface nitridation) | $H_2$ | 900(nitridation temperature)<br>1100 (growth temperature | 20 torr | Good epitaxy achieved | [61] |
| Pulse mode injection of precursors Triethylamine borane and ammonia | C-plane sapphire substrate | $H_2$ | 1350 | 10 torr | Different pulse time was tried, and optimum parameter was achieved | [77] |
| Triethyl borane and ammonia (V/III ratio varied between 2000 and 4000) | Sapphire substrate | Carrier gas flow rate was varied ($H_2$) | Buffer layer at ~600-800.<br>Main epilayer ≥1400 | Not mentioned | 380 arcsec FWHM with excellent stoichiometric ratio and surface morphology | [77]-[82] |

| | | | | | | | |
|---|---|---|---|---|---|---|---|
| Same precursor was used with a varied $NH_3$ injection rate | Sapphire substrate | $H_2$; 27 slm | 1000 | | 3.85 kPa | Effect of $NH_3$ injection rate was observed and optimized | [78] |

## 2.2 h-BN Device fabrication processes:

To formulate the MSM detector device structures, freestanding h-BN layers are needed. Freestanding device layers can be obtained by the mechanical exfoliation process [79,80]. After the exfoliation process, films are diced into desired dimensions. Figure 4 shows the schematic of vertical and lateral devices. Metal contacts are formed as anode and cathode using a metallization process using e-beam evaporation. Different bilayer metal contacts have been deployed to measure device performance. Table 5 shows some of the physical parameters of devices. In the traditional room temperature semiconductor-based radiation detector material CdZnTe, a different type of device and electrode geometry has been implemented. In the case of h-BN, most of the works are based on planar MSM geometry.

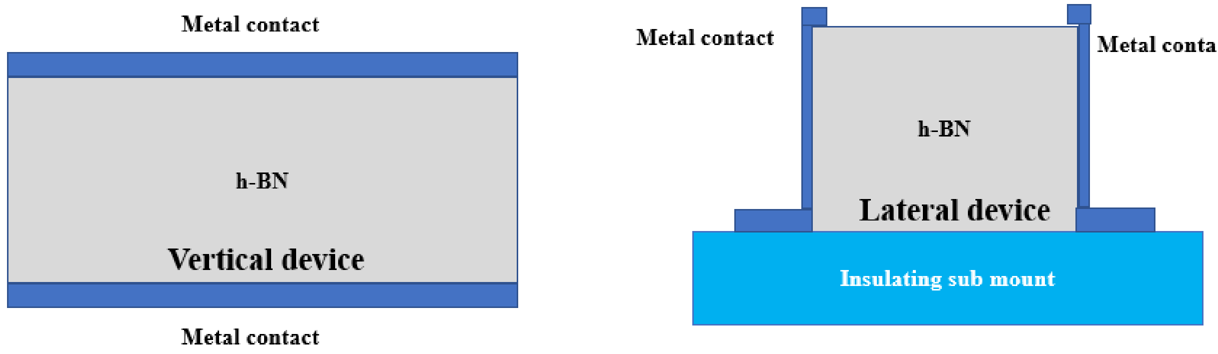

Figure 4. Cross-sectional schematic of lateral and vertical MSM neutron detector [74], [82]

### 2.2.1 Etching:

The etching of h-BN requires external energy as an enabling agent to initiate and sustain the removal of surface atoms. The external energy can be in the form of ion bombardment in reactive ion etching (RIE). The bombardment of surfaces with ions can cause damage. RIE/selective RIE, with an emphasis on low damaged processes, has been investigated. Inductively coupled plasma reactive ion etching (ICP-RIE) using various gas mixtures of $BCl_3/SF_6/O_2$ at low plasma-induced voltages (<60 V) has been employed by different groups [18], [77]–[81].

### 2.2.2 Ohmic contacts:

There are limited works regarding ohmic contact formation on h-BN MSMs [77–81]. The reports start with Ti/Al metallization. Annealing Ti/Al without any overlayer, even in a full nitrogen environment, still produces a lot of surface oxides, which degrades contact resistance and

doi:10.20944/preprints202204.0297.v1

makes the probe contacts nearly impossible. This has necessitated studies on Ti/Al-h-BN-Ti/Al, Ti/Al-h-BN-Ni/Au, Ni/Au-h-BN-Ti/Al, Ni/Au-h-BN-Ni/Au, Ti/Ti-h-BN-Ti/Ti based contacts. Essential attributes of ohmic contact formation are low contact resistance, high edge acuity, low surface roughness, minimal lateral diffusion, and thermal stability. Doan *et al*. reported that Ni/Au-h-BN-Ni/Au is the best suitable contact material for h-BN based detectors with the highest efficiency. [18,31,79–83]

In order to reduce the Ohmic contact area and check the efficiency variation, lateral devices have been deployed. The reported lateral devices use Ni/Au bilayer metal contacts varying the anode to cathode distance.

Table 5: Device physical parameters

| No | Material thickness | Contact type | Device type | Area of the device | Ref. |
|---|---|---|---|---|---|
| 1 | 0.3 µm | Ti/Al | Lateral | 4.8 mm$^2$ | [18] |
| 2 | 0.3 µm | Ti/Al | Lateral | 12 mm$^2$ | [83] |
| 3 | 0.3-43 | Ti/Al | vertical | Not mentioned | [82] |
| 4 | 43 µm | Ni/Au | vertical | 1 mm$^2$ | [79] |
| 5 | 2.5-15 µm | Ti/Ti | vertical | 40mm$^2$ -14mm$^2$ | [81] |
| 6 | 50 µm | Ni/Au | Vertical | 9 mm$^2$ | [80] |
| 7 | 50 µm | Ni/Au and Ti/Al | vertical | 1 mm$^2$ | [76] |
| 8 | 90 µm | Ni/Au | Lateral | 29 mm$^2$ | [84] |
| 9 | 100 µm | Ni/Au | Lateral | 1 cm$^2$ | [85] |

### 2.3 Experimental setup:

High-density polyethylene (HDPE) moderator is usually used for the neutron measurement experimental setup purpose with a Californium-252 ($^{252}$Cf) neutron source. The moderator is used to contain radioactive material as well as to convert fast neutrons to thermal neutrons. There are two holes, A and B, where hole A housed the source when in use and hole B housed the source when the measurement was completed. Hole B is much closer to the detector to increase the thermal neutron flux. The fabricated h-BN detector is usually placed at a certain distance away from the neutron source and covered with Al foil to reduce electronic noise. Readout electronics are used to quantify the signal from the detector [18,79]. A schematic of the experimental setup is shown in Figure 5.

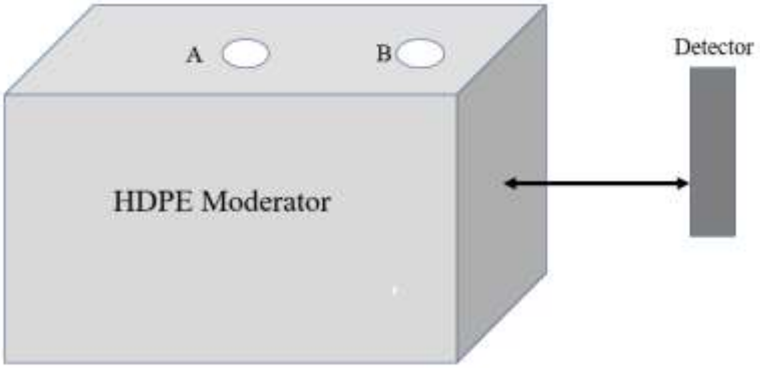

Figure 5: Experimental setup schematic for neutron absorption measurement. [18,79]

There are several ways of building readout electronics [86,87]. The basic circuitry consists of a body of h-BN with two electrodes connected, described as anode and cathode. The electrodes need to be perpendicular to the crystallographic axis of the h-BN. A high electric field needs to be applied parallel to the crystallographic axis of h-BN. The neutron flux is exposed to the device from a certain distance, and produced current pulse is measured. To measure the signal, a charge sensitive amplifier, a pulse shaping amplifier is being connected to a multichannel analyzer (MCA), as shown in the schematic in Figure 6.

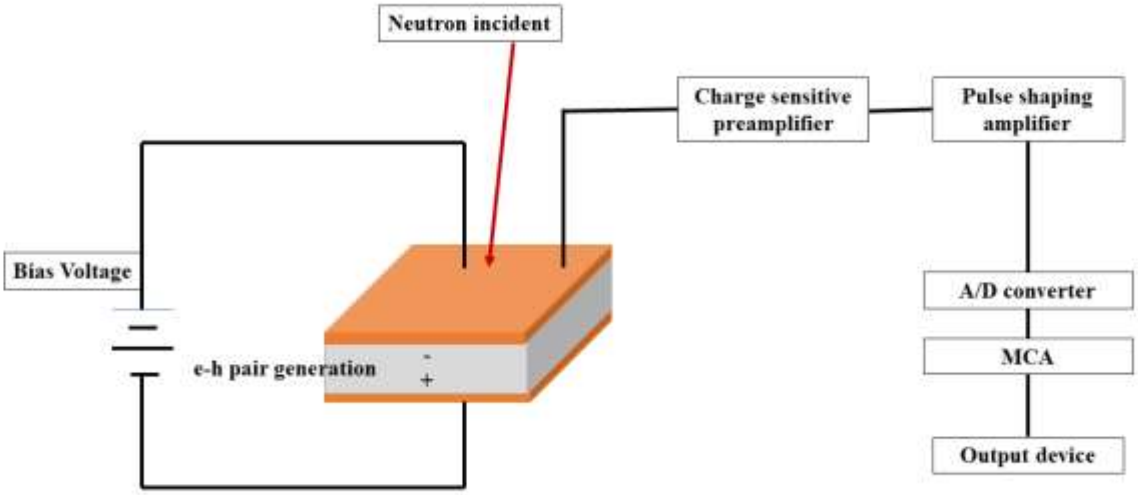

Figure 6: Schematic for the readout electronics [83,87]

## 3. Results and Discussions:

### 3.1 Point defect issues:

h-BN growth temperature is very high. So, oxygen and carbon impurities can occupy nitrogen sites denoted as $O_N$ and $C_N$ respectively (subscript N means nitrogen atom). As shown in Figure 1, h-BN has a weak van der Waals force between its' layers. So, it tends to peel off automatically or due to mechanical force from its substrate. It has been reported that $O_N$ and $C_N$ impurities are more common near the interface of h-BN and sapphire substrate (bottom surface) compared to the top surface of h-BN. It is important to choose which side of the grown device needs to be exposed to neutron absorption. Figure 7 shows a schematic of two different cases in vertical detectors. In case (a), a neutron is incoming through the top surface. After the incidence, it decays based on the exponential decay formula ( $I = I_0 e^{(-x/\chi)}$ ). In case 2, the device is made such that neutron is coming through the bottom surface. It shows that the choice of incidence orientation has an impact on neutron absorption. The top surface as a neutron incident interface is favorable as it has less $O_N$ . Biasing voltage polarity is another important parameter to consider. In vertical devices, positive on the top surface or vice versa is implemented and tested. Du *et al*. showed that changing carrier gas to more passive nitrogen gas can decrease oxygen and carbon occupancy in nitrogen sites [88,89].

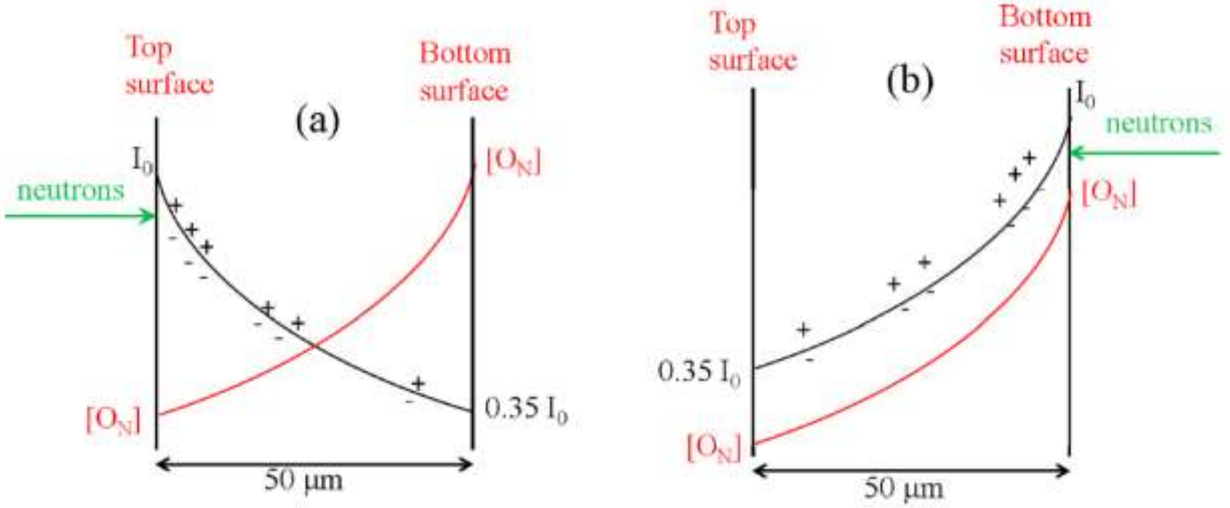

Figure 7: Schematic of oxygen occupancy in nitrogen sites with neutron incidence direction [The figure is reproduced from [76] with permission from AIP Publishing]

### 3.2 Ohmic contacts:

Ohmic contact formation is another essential aspect to consider. The performance of the device largely depends on charge collection efficiency. The derived signal is amplified, integrated, and finally digitized to characterize using MCA. The presence of any kind of noise reduces the chance of detecting the original signal. The most common type of noise is 'shot noise', which largely depends on the leakage current of the device [90]. Different type of ohmic contacts has been researched, as mentioned in Table 5. In the case of vertical devices, Ni/Au has been tested as the best one with the highest efficiency and low leakage current. Most of the other works also follow the same Ni/Au based ohmic contacts.

### 3.3 Epilayer thickness and absorption length

Diffusion lengths for Li and alpha particles are between 2 μm to 5 μm. So, if the material thickness is good enough, the Li and alpha particles are confined inside the detector material. Neutron absorption follows the below formula,

$$n_{abs} = \Phi_1 A(1 - e^{-d/\chi})t \qquad (3)$$

where $t$ is total counting time, d is the thickness of h-BN epilayer, A is the cross-sectional area, $n_{abs}$ is neutron count, $\Phi_1$ is the neutron flux, and $\chi$ is the thermal neutron absorption length. Thus, the thickness of the material is a critical parameter. The material thickness needs to be higher than the neutron absorption length. Thickness dependent data is shown in Figure 8 [18].

Boron density in h-BN is $5\times10^{22}$ $cm^{-3}$ where 20% is $^{10}B$, and 80% is $^{11}B$. So, the density of $^{10}B$ is around $N=1.1\times10^{22}$ $cm^{-3}$. Neutron absorption coefficient, $\alpha_{natural} = N\sigma = 42.24$ $cm^{-1}$ and absorption length, $\chi_{natural} = 1/\alpha_{natural} = 2.37\times10^{-2}$ cm where $N = 1.1\times10^{22}$ $cm^{-3}$ and $\sigma = 3.84\text{x}10^{-21}$ $cm^2$ is the cross-section for $^{10}B$ for thermal neutron (25.3meV) [18]. If we can increase the amount of $^{10}B$ percentage in h-BN, then absorption length will decrease. In the case of 100% $^{10}B$ enriched h-BN, the absorption length reduces to 47.3 μm [79]. Li *et al.* showed interesting experimental data in their paper, which shows the relationship between h-BN layer thickness and relative neutron transmission which is shown in Figure 8. They measured that the neutron absorption length for natural h-BN is around 277 μm, close to the theoretical value of 237 μm [31]. The electron-hole (e-h) pair generation energy is approximately three times of bandgap [36]. Thus, as per equation 3, the neutron absorption process creates an average of 2.34 MeV energy, which corresponds to 1.3 $\text{x}10^5$ electron-hole (e-h) pairs generation [31]. As the thickness of the epilayer increases, the radiative neutron transmission rate decreases, which means more neutrons are absorbed inside the material. Thus, the probability of electron-hole pair creation increases.

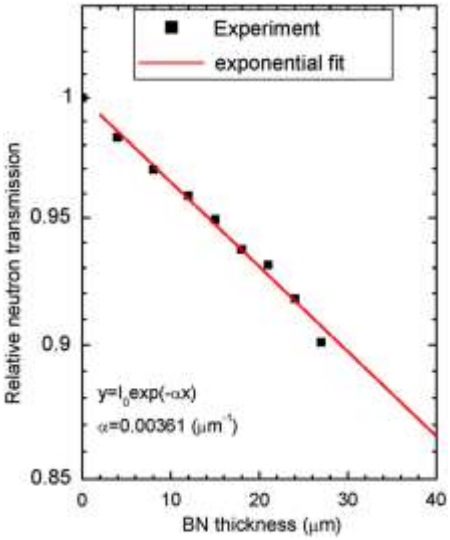

Figure 8. Neutron transmission dependency on h-BN epilayer thickness [The image is reproduced from [31] with permission from Elsevier]

### 3.4 Mobility lifetime product:

The absorbed neutrons create electron-hole (e-h) pairs in the semiconductor materials, which produce a detectable signal. It is essential to collect the e-h pairs generated through nuclear reaction before recombination. For this, carrier transit time ($\tau_t$) must be smaller than the e-h pair recombination time ($\tau$) [18]. The relationship is as below:

$$\tau_t = \frac{L}{\mu E} = \frac{L^2}{\mu V} \qquad (4)$$

Where V is the applied bias voltage, E is the electric field, and L is the distance between electrodes. Most of the electrons can be collected if the below relation holds considering $\tau_t < \tau$,

$$\tau\mu > \frac{L^2}{V} = \frac{LA}{\rho I} \qquad (5)$$

where $\rho$ is the resistivity of the material, I is the generated current in the external circuit, and A is the cross-sectional area. Mobility lifetime product thus depends on device geometry, material quality, and as well as material resistivity. If the quality of the material is better, so is the resistivity, then the mobility lifetime product becomes much higher. Doan *et al*. showed some of the measured results for their fabricated device. They showed that under a certain value, neutron detection capability degrades [18]. Figure 9 (a) shows their derived results for certain device geometry.

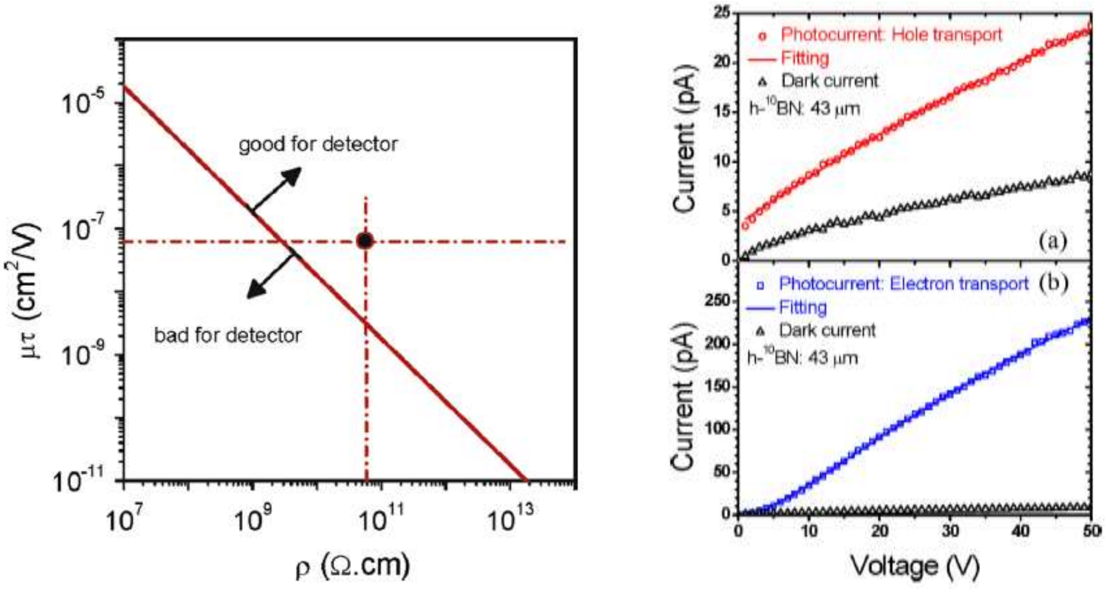

a) b)

Figure 9: a) mobility-life time product versus resistivity, b) fitting of Many's equation to get $\mu\tau$ product [Figure (a) is reproduced from [18] with permission from Elsevier, and Figure (b) is reproduced from [79] with permission from AIP publishing]

Now the question arises, how to measure this mobility lifetime product of the fabricated device. All the published paper in this field follows Many's equation to calculate this parameter from the photocurrent characteristics under illumination curve fitting (as an example in Figure 9(b)) [91]:

$$I_i(V) = I_{o,i}\eta_{c,i} = I_{o,i}\left(\frac{\mu_i\tau_i V\left(1-e^{-\left(\frac{L^2}{\mu_n\tau_n V}\right)}\right)}{L^2\left(1+\frac{s_i L}{\mu_i V}\right)}\right), i = e, h \qquad (6)$$

Where $\eta_c$ is the charge collection efficiency, $I_o$ is the saturation current, i=e denoted parameter for electron, i=h denotes parameters for holes $S_i$ is the surface recombination velocity, where $E_s=S_i/\mu$ ($\mu$ is the mobility and $E_s$ is the applied electric field), $V_b=V$ is the bias voltage applied between electrodes to accelerate charge carriers, which leads to an applied electric field as $E_a=V/L$ where L is the distance between electrodes. Many's equation implies that to get better charge collection efficiency, a) carrier drift length needs to be larger than transit distance, which is the same as equation 6, b) the external applied field needs to be larger than the surface recombination field to collect the charges from the detector [92]. From Doan *et al*., the better the h-BN quality, the higher the resistivity, the higher the $\tau\mu$ product is, so is the detector efficiency and sensitivity [18,82,83]. Maity *et al*. have reported $\tau_i\mu_i$ product much higher for holes compared to electrons, which contradicts some other reports [79]. Cao *et al*. have reported that electron and hole effective mass in h-BN single sheet is the same as their mobility [93]; thus, , a higher $\tau_i\mu_i$ for holes means $\tau_h >> \tau_e$. This is also one of the proofs that undoped h-BN's quasi-Fermi level is below the intrinsic Fermi level, which means the material is naturally p-type [18,83]. Maity *et al*. showed in their report that considering the hole transport characteristics and device size, the resistivity of 43, 50, and 100 μm thick h-BN film is ~$10^{13}$ ohm-cm [76,80,84,85].

### 3.5 Pulse height spectra and energy resolution:

With a certain applied electric field, all the charge carriers are collected via electrodes. This signal is then pre-amplified, then pass through a gaussian shaped amplifier, and read via MCA. Doan *et al*. mentioned that FWHM of Li and alpha particle peaks in MCA in the case of MSM h-BN detectors is less compared to boron coated semiconductor detectors [12,18,94]. So, the energy resolution is much better for MSM detectors. The channel number vs. count data from MCA is resolved by fitting the data against energy product vs. channel number, as shown in Figure 10 [83]. It has been reported that the data becomes more resolved if the material quality is much better with fewer charge carrier traps, fewer defects, higher $\mu\tau$ products, and obviously, the material thickness need to be much higher than the absorption length of Li and alpha particles (2-5 μm). The energy resolution of h-BN based detectors has been reported much better compared to $^{10}$B perforated Si pillar based indirect conversion detectors as Li and alpha particle absorption lengths are random due to charge carrier traps [16,95–97]. The charge carrier trap issue is severe in polycrystalline materials.

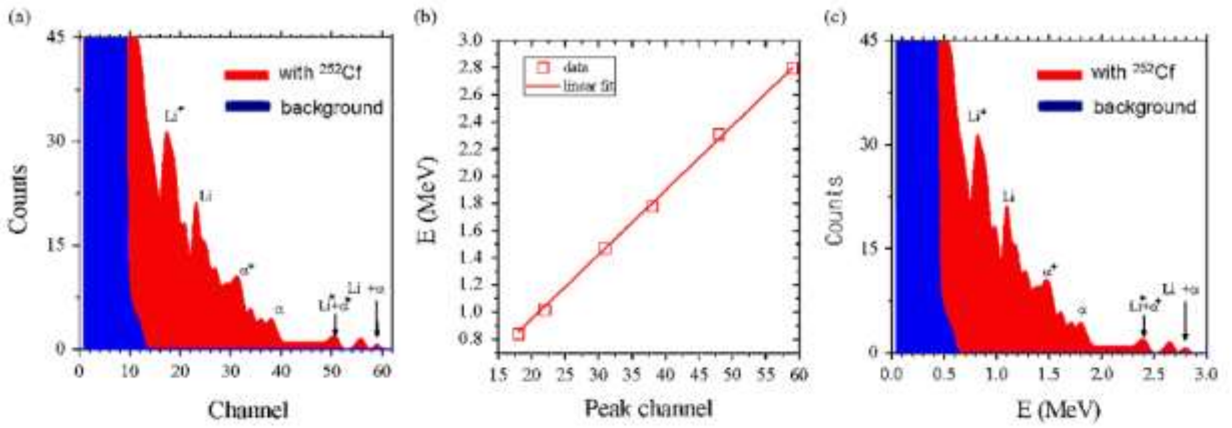

Figure 10. (a) Counts versus channel number, (b) energy peak calibration among all expected nuclear reaction products, and (c) counts vs. energy (MeV) [The figures are reproduced from [83] with permission from Elsevier]

In Figure 10 (a) and (c), the blue column bars are the measured counts in the absence of $^{252}C_{f(}$source), which is just the background noise. The red column bars are the measured counts in the presence of the $^{252}C_{f(}$source). As mentioned in equations (1) and (2), the peak positions in Figure 10(c) show the energy corresponding to Li, Li*, α, and α* peaks, as well as the sum peaks Li+α and Li*+α*. Figure 10(b) shows the linear relationship between the corresponding energy and MCA channel number.

### 3.6 Device efficiency:

h-BN detectors in the reports are calibrated against a commercially purchased neutron detector. Maity *et al*. reported a comparison with a $^{6}$LiF neutron detector with 33% efficiency. The neutrons count rate per unit area for h-BN and commercially purchased detectors are 77.2 and 45.1 n/s-cm$^{2}$. Using the detection ratio, the authors calculated the efficiency of the h-BN detector was 51.4%. And the Charge Collection Efficiency (CCE) at a bias voltage of 400V was about 86.1 %. The other parameters affecting the efficiency and sensitivity of the detector are the limitation of detector area and radioactive material to detector distance [79]. All the results so far have been derived and are based on natural $^{10}$B in h-BN. It has been proposed to use enriched $^{10}$B to increase the amount of neutron absorbing cross-section in the semiconductor material. In the case of vertical devices, the highest device area was achieved by Maity et al. as 90 mm$^{2}$ with 90 μm epilayer thickness and 50 percent efficiency [84]. Another detector has been reported by Maity *et al*. with 58 % efficiency with 50 μm thickness, but the device area is very small (1 mm$^{2}$) [76]. Distance from the device to detector material is also a point of consideration. It has an inverse-square relation with neutron flux [18].

Charge collection efficiency (CCE) is a very important parameter. It can be defined as CCE=$\eta_{coll} = \dfrac{\eta}{P} = \dfrac{N_c / N_{in}}{t / \chi}$ where $N_c$ is the measured neutron counts, and $N_{in}$ is the total neutron counts, t is the thickness of the sample, $\chi$ is the thermal neutron absorption length, and $P$ is the probability of interaction. It has been previously described that $\chi$ =237 μm. So, such thicker defect-free single-crystal h-BN has not been reported yet. That is why interaction probability cannot reach 100%. So far, the maximum thickness has been reported as 100 μm; in that case, $P$ is around 37.8%. The reported maximum charge collection efficiency is 86%. Alpha particle absorption is directly proportional to the h-BN layer thickness [96]. h-BN is a graphite-like layered material where the interlayer distance is around 3.33 nm. It has been reported that five e-h pairs are usually generated in each interlayer [96].

### 3.7 Lateral vs. Vertical devices:

Scaling up the neutron detector is very important from the commercialized application point of view. The 58% detection efficiency with a 1 mm$^2$ device back in 2017 has very low neutron flux, which is around 3x10$^5$ neutrons/s. The problem with vertical devices is if the device area is scaled up, then efficiency and CCE decrease, but the leakage current increases. Due to the increase in the ohmic contact area, capacitance and surface recombination increase, ultimately lowering the CCE and efficiency [92]. The opposite has been demonstrated in the lateral device with a 29 mm$^2$ device size with 50% efficiency. The interesting point is that the mobility-lifetime product is higher compared to previously reported data. In-plane mobility has been reported as 100 times more than vertical mobility, which leads to higher CCE [92]. Resistivity is lower in the case of lateral devices, but due to less contact area, surface recombination is less. So, leakage current and CCE are higher. As the contact area is significantly reduced in the case of lateral devices, the capacitance and RC time constant are also reduced. Surface trap states are reduced in the case of lateral devices due to less contact area. All these effects eventually lead to a high-efficiency detector with a higher surface area.

The most recent report regarding lateral device geometry mentioned 1 cm$^2$ device with 59% detection efficiency. The device thickness is 100 μm. The significant improvement of material thickness and quality has resulted in 6 times increase in mobility lifetime product and 3 times decrease in surface recombination field [85]. It is so far the best device data that has been demonstrated.

Table 6. Summary of the results found in different references.

| No. | Material thickness in µm | $\mu\tau$ for electrons | $\tau\mu$ for holes | resistivity | Material Specimen in mCi | Area of the device in mm$^2$ | bias voltage in V | time measured | Distance from detector in cm | Efficiency | Reference |
|---|---|---|---|---|---|---|---|---|---|---|---|
| 1 | 0.3 | 4.5x10$^{-8}$ | 7.1x10$^{-9}$ | 5.3x10$^{10}$ | 2.4 | 4.8 | 240 | 26h | 3 | Not mentioned | [18] |
| 2 | 0.3 | 2.83x10$^{-7}$ | 2.83x10$^{-7}$ | 5.0x10$^{10}$ | 1.6 | 12 | 20 | Not mentioned | 12 | Not mentioned | [83] |
| 3 | 0.3-43 | 3.3x10$^{-7}$ | 3.3x10$^{-7}$ | 5.0x10$^{10}$ | Not mentioned | Not mentioned | Variable | 20 min | 9 | 51.40% (43 µm) | [82] |
| 4 | 43 | 8.3x10$^{-7}$ | 2.2x10$^{-5}$ | 1.0x10$^{13}$ | 0.93 | 1 | 400 | 10 min | 30 | 51.40% | [79] |
| 5 | 2.5-15 | 3.0x10$^{-7}$ | 5.0x10$^{-8}$ | 3.0x10$^{9}$ | Not mentioned | 14-40 | 700, 450, 600, 700 | Not mentioned | 8 | 4.21-21.37% | [81] |
| 6 | 50 | 2.0x10$^{-6}$ | 1.0x10$^{-5}$ | 1.0x10$^{13}$ | 0.77 | 9 | 200 | 15 min | 57.5 | 53% | [80] |
| 7 | 50 | 1.0x10$^{-6}$ | 1.0x10$^{-6}$ | Not mentioned | Not mentioned | 1 | 200 | Not mentioned | 27.5 | 58% | [76] |
| 8 | 90 | 1.0x10$^{-4}$ | 1.0x10$^{-4}$ | Not mentioned | 0.5 | 29 | 400 | 15min | 60 | 50% | [84] |
| 9 | 100 | 5.0x10$^{-3}$ | 5.0x10$^{-3}$ | 1.0x10$^{12}$ | 0.45 | 100 | 500 | 15 min | Not mentioned | 59% | [85] |

## Conclusions:

MSM detectors based on h-BN have been mainly being researched for the last ten years, and still, it is a premature technology. The challenge regarding fewer defects and thicker material growth has been addressed. Still, the oxygen occupancy issue needs to be solved. In all the previous works, the MOCVD growth of h-BN is done on sapphire. As h-BN growth is a high-temperature process, oxygen occupancy near the substrate has not been solved. One solution can be to grow some other type of template material like AlN. Then grow h-BN on top of the AlN buffer layer. In that case, the oxygen vacancy issue can be addressed. This hypothesis has not been tested yet. The neutron absorption length for h-BN is 237 µm. So far, material up to 100 µm has been grown, and the detector is being fabricated to get high efficiency. More than 100 µm thickness has not been reported yet. Though vertical and lateral types have been reported, the maximum efficiency has been reported for lateral devices with 59% and 1cm$^2$ device area. Vertical devices have also shown good neutron detection efficiency (58%) and CCE (86%) but suffer from low device area, leading to less neutron flux absorption. Vertical devices have shown lower mobility as well as lower mobility-lifetime product, higher surface recombination field due to higher surface traps, higher capacitance due to higher contact area, and, as mentioned before, can capture less neutron flux. All these parameters reduce device sensitivity. It has been shown that the lateral device is a better option to increase the device area, but there is a tradeoff between efficiency and area. In the case of the lateral device, mobility lifetime product has been increased, leakage current, capacitance, and surface recombination effect have been decreased. Not that much work has been done regarding the metal contacts. More attention is required in this field to reduce the leakage current. This might have an implication on overall device performance. h-BN based neutron detectors can be very promising, but the commercial implementation still needs lots of R&D based work in the coming days to be used in real-life application.

## Acknowledgements:

This work was supported by the National Science Foundation (NSF) award No. 2124624 managed by Dr. Dominique M. Dagenais and SCEEE research initiation grant for 2021-2022.

## References:

1. US Department of Energy DOE FUNDAMENTALS HANDBOOK NUCLEAR PHYSICS Volume 2 of 2. *Nucl. Phys.* **1993**, *1*, 36, doi:DOE-HDBK-1019/2-93.
2. McGregor, D. S., Klann, R. T., Gersch, H. K., & Yang, Y. H.. Thin-film-coated bulk GaAs detectors for thermal and fast neutron measurements. Nuclear Instruments and Methods in Physics Research Section A: Accelerators, Spectrometers, Detectors and Associated Equipment, 466(1), 126-141. 2001.
3. Coleman, R. THE APPLICATION OF NEUTRON ACTIVATION ANALYSIS TO FORENSIC SCIENCE. **1967**.
4. AH Youmans - US Patent 2, 760,078;, *Conduction Counter for Radioactivity Well Logging*; **1956**
5. Yazbeck, J. Investigations of Hexagonal Boron Nitride As a Semiconductor For. *Energy* **2012**.
6. Caruso, A.N. The Physics of Solid-State Neutron Detector Materials and Geometries. *J. Phys.*

*Condens. Matter* **2010**, *22*, doi:10.1088/0953-8984/22/44/443201.

7. Salt, C.; Lennox, A.J.; Takagaki, M.; Maguire, J.A.; Hosmane, N.S. Boron and Gadolinium Neutron Capture Therapy. *Russ. Chem. Bull.* **2004**, *53*, 1871–1888, doi:10.1007/s11172-005-0045-6.
8. Knoll, G. Radiation Detection and Measurement, 3rd Ed - Glenn F **2009**, 1–796.
9. Kouzes, R.T.; Ely, J.H.; Erikson, L.E.; Kernan, W.J.; Lintereur, A.T.; Siciliano, E.R.; Stephens, D.L.; Stromswold, D.C.; Van Ginhoven, R.M.; Woodring, M.L. Neutron Detection Alternatives to 3He for National Security Applications. *Nucl. Instruments Methods Phys. Res. Sect. A Accel. Spectrometers, Detect. Assoc. Equip.* **2010**, *623*, 1035–1045, doi:10.1016/j.nima.2010.08.021.
10. Angelone, M. Neutron Detection : Principles , Methods , Issues ( and Tips ) Maurizio Angelone. *October* **1989**.
11. McGregor, D. S., & Shultis, J. K.. Spectral identification of thin-film-coated and solid-form semiconductor neutron detectors. Nuclear Instruments and Methods in Physics Research Section A: Accelerators, Spectrometers, Detectors and Associated Equipment, 517(1-3), 180-188. **2004**.
12. Nikolic, R.J.; Cheung, C.L.; Li; Reinhardt, C.E.; Wang, T.F. Roadmap for High Efficiency Solid-State Neutron Detectors. *spiedigitallibrary.org* **2005**, *15*, 601305, doi:10.1117/12.633256.
13. Nikolic, R. J., Conway, A. M., Reinhardt, C. E., Graff, R. T., Wang, T. F., Deo, N., & Cheung, C. L. Pillar structured thermal neutron detector with 6: 1 aspect ratio,”. In Appl. Phys. Lett. **2008**.
14. Bellinger, S. L., Fronk, R. G., McNeil, W. J., Sobering, T. J., & McGregor, D. S. (2011). Enhanced variant designs and characteristics of the microstructured solid-state neutron detector. Nuclear Instruments and Methods in Physics Research Section A: Accelerators, Spectrometers, Detectors and Associated Equipment, 652(1), 387-391, **2011**.
15. Clinton, J. Optimization and Characterization of a Novel Self Powered Solid State Neutron Detector. **2011**.
16. Shao, Q.; Voss, L.F.; Conway, A.M.; Nikolic, R.J.; Dar, M.A.; Cheung, C.L. High Aspect Ratio Composite Structures with 48.5% Thermal Neutron Detection Efficiency. *Appl. Phys. Lett.* **2013**, *102*, doi:10.1063/1.4792703.
17. Osberg, K., Schemm, N., Balkir, S., Brand, J. I., Hallbeck, M. S., Dowben, P. A., & Hoffman, M. W.. A handheld neutron-detection sensor system utilizing a new class of boron carbide diode. IEEE Sensors Journal, 6(6), 1531-1538. **2006**.
18. Doan, T.C.; Majety, S.; Grenadier, S.; Li, J.; Lin, J.Y.; Jiang, H.X. Fabrication and Characterization of Solid-State Thermal Neutron Detectors Based on Hexagonal Boron Nitride Epilayers. *Nucl. Instruments Methods Phys. Res. Sect. A Accel. Spectrometers, Detect. Assoc. Equip.* **2014**, *748*, 84–90, doi:10.1016/j.nima.2014.02.031.
19. Jiang, H. X., & Lin, J. Y. (2016). Hexagonal boron nitride epilayers: growth, optical properties and device applications. ECS Journal of Solid State Science and Technology, 6(2), Q3012, **2016**.
20. Huang, K.C.; Dahal, R.; Lu, J.J.Q.; Weltz, A.; Danon, Y.; Bhat, I.B. Scalable Large-Area Solid-State Neutron Detector with Continuous p-n Junction and Extremely Low Leakage Current. *Nucl. Instruments Methods Phys. Res. Sect. A Accel. Spectrometers, Detect. Assoc. Equip.* **2014**, *763*, 260–265, doi:10.1016/j.nima.2014.06.047.
21. Shultis, J. K., & McGregor, D. S.. Design and performance considerations for perforated semiconductor thermal-neutron detectors. Nuclear Instruments and Methods in Physics Research Section A: Accelerators, Spectrometers, Detectors and Associated Equipment, 606(3), 608-636, **2009**.

22. McGregor, D. S., & Shultis, J. K.. Spectral identification of thin-film-coated and solid-form semiconductor neutron detectors. Nuclear Instruments and Methods in Physics Research Section A: Accelerators, Spectrometers, Detectors and Associated Equipment, 517(1-3), 180-188. **2004**.
23. McGregor, D. S., Hammig, M. D., Yang, Y. H., Gersch, H. K., & Klann, R. T.. Design considerations for thin film coated semiconductor thermal neutron detectors—I: basics regarding alpha particle emitting neutron reactive films. Nuclear Instruments and Methods in Physics Research Section A: Accelerators, Spectrometers, Detectors and Associated Equipment, 500(1-3), 272-308. **2003**.
24. Gersch, H. K., McGregor, D. S., & Simpson, P. A. . The effect of incremental gamma-ray doses and incremental neutron fluences upon the performance of self-biased 10B-coated high-purity epitaxial GaAs thermal neutron detectors. Nuclear Instruments and Methods in Physics Research Section A: Accelerators, Spectrometers, Detectors and Associated Equipment, 489(1-3), 85-98. **2002**.
25. Dahal, R.; Huang, K.C.; Clinton, J.; Licausi, N.; Lu, J.Q.; Danon, Y.; Bhat, I. Self-Powered Micro-Structured Solid State Neutron Detector with Very Low Leakage Current and High Efficiency. *Appl. Phys. Lett.* **2012**, *100*, doi:10.1063/1.4729558.
26. McGregor, D. S., Klann, R. T., Gersch, H. K., & Yang, Y. H. . Thin-film-coated bulk GaAs detectors for thermal and fast neutron measurements. Nuclear Instruments and Methods in Physics Research Section A: Accelerators, Spectrometers, Detectors and Associated Equipment, 466(1), 126-141, **2001**.
27. Rose, A.. Sputtered boron films on silicon surface barrier detectors. Nuclear Instruments and Methods, 52(1), 166-170, **1967**.
28. FP Doty - US Patent 6, 727,504; **2004**, *Boron Nitride Solid State Neutron Detector*;
29. Doty, F. Boron Nitride Solid State Neutron Detector. **2004**.
30. McGregor, D. S., Unruh, T. C., & McNeil, W. J.. Thermal neutron detection with pyrolytic boron nitride. Nuclear Instruments and Methods in Physics Research Section A: Accelerators, Spectrometers, Detectors and Associated Equipment, 591(3), 530-533. **2008**.
31. Li, J.; Dahal, R.; Majety, S.; Lin, J.Y.; Jiang, H.X. Hexagonal Boron Nitride Epitaxial Layers as Neutron Detector Materials. *Nucl. Instruments Methods Phys. Res. Sect. A Accel. Spectrometers, Detect. Assoc. Equip.* **2011**, *654*, 417–420, doi:10.1016/j.nima.2011.07.040.
32. Hongxing Jiang, Jingyu Lin, Jing Li, Avisek Maity, Sam Grenadier, US20200135958A1. 2018.
33. Nava, F.; Bertuccio, G.; Cavallini, A.; Vittone, E. Silicon Carbide and Its Use as a Radiation. **2008**, doi:10.1088/0957-0233/19/10/102001.
34. del Sordo, S.; Abbene, L.; Caroli, E.; Mancini, A.M.; Zappettini, A.; Ubertini, P. Progress in the Development of CdTe and CdZnTe Semiconductor Radiation Detectors for Astrophysical and Medical Applications. *Sensors* **2009**, *9*, 3491–3526, doi:10.3390/s90503491.
35. Laturia, A.; Van de Put, M.L.; Vandenberghe, W.G. Dielectric Properties of Hexagonal Boron Nitride and Transition Metal Dichalcogenides: From Monolayer to Bulk. *npj 2D Mater. Appl.* **2018**, *2*, 1–7, doi:10.1038/s41699-018-0050-x.
36. Goudsmit, S.A. Physical Review Letters: Editorial. *Phys. Rev. Lett.* **1960**, *5*, 233, doi:10.1103/PhysRevLett.5.233.
37. Li, J.; Majety, S.; Dahal, R.; Zhao, W.P.; Lin, J.Y.; Jiang, H.X. Dielectric Strength, Optical Absorption, and Deep Ultraviolet Detectors of Hexagonal Boron Nitride Epilayers. *Appl. Phys. Lett.* **2012**, *101*, doi:10.1063/1.4764533.

38. Majety, S.; Li, J.; Cao, X.K.; Dahal, R.; Lin, J.Y.; Jiang, H.X. Metal-Semiconductor-Metal Neutron Detectors Based on Hexagonal Boron Nitride Epitaxial Layers. *spiedigitallibrary.org* **2012**, doi:10.1117/12.940748.
39. Grenadier, S.; Li, J.; Lin, J.; Jiang, H. Dry Etching Techniques for Active Devices Based on Hexagonal Boron Nitride Epilayers ARTICLES YOU MAY BE INTERESTED IN. *Cite as J. Vac. Sci. Technol. A* **2013**, *31*, 61517, doi:10.1116/1.4826363.
40. Majety, S.; Cao, X.K.; Dahal, R.; Pantha, B.N.; Li, J.; Lin, J.Y.; Jiang, H.X. Semiconducting Hexagonal Boron Nitride for Deep Ultraviolet Photonics. *spiedigitallibrary.org* **2012**, doi:10.1117/12.914084.
41. Li, J.; Gui, G.; Zhong, J. Tunable Bandgap Structures of Two-Dimensional Boron Nitride. *J. Appl. Phys.* **2008**, *104*, 1–6, doi:10.1063/1.3006138.
42. Pacilé, D.; Meyer, J.C.; Girit, Ç.Ö.; Zettl, A. Cite As. *Appl. Phys. Lett* **2008**, *92*, 133107, doi:10.1063/1.2903702.
43. Li, L.; Chen, Y.I.; Zhang, H.; Li, L.H.; Chen, Y.; Behan, G.; Petravic, M.; Glushenkov, A.M. Large-Scale Mechanical Peeling of Boron Nitride Nanosheets by Low-Energy Ball Milling Large-Scale Mechanical Peeling of Boron Nitride Nanosheets by Low-Energy Ball Milling †. *Artic. J. Mater. Chem.* **2011**, doi:10.1039/c1jm11192b.
44. Coleman, J. N., Lotya, M., O'Neill, A., Bergin, S. D., King, P. J., Khan, U., & Nicolosi, V.. Two-dimensional nanosheets produced by liquid exfoliation of layered materials. Science, 331(6017), 568-571, **2011**.
45. Lin, Y., Williams, T. V., & Connell, J. W.. Soluble, exfoliated hexagonal boron nitride nanosheets. The Journal of Physical Chemistry Letters, 1(1), 277-283. **2010.**
46. Han, W.Q.; Wu, L.; Zhu, Y.; Watanabe, K.; Taniguchi, T. Structure of Chemically Derived Mono- and Few-Atomic-Layer Boron Nitride Sheets. *Appl. Phys. Lett.* **2008**, *93*, doi:10.1063/1.3041639.
47. Zhi, C.; Ueda, S.; Zeng, H.; Wang, X.; Tian, W.; Wang, X.; Bando, Y.; Golberg, D. Weak Morphology Dependent Valence Band Structure of Boron Nitride. *J. Appl. Phys.* **2013**, *114*, doi:10.1063/1.4817430.
48. Jin, C.; Lin, F.; Suenaga, K.; Iijima, S. Fabrication of a Freestanding Boron Nitride Single Layer and Its Defect Assignments. *APS* **2009**, *102*, doi:10.1103/PhysRevLett.102.195505.
49. Warner, J.H.; Rümmeli, M.H.; Bachmatiuk, A.; Büchner, B. Atomic Resolution Imaging and Topography of Boron Nitride Sheets Produced by Chemical Exfoliation. *ACS Nano* **2010**, *4*, 1299–1304, doi:10.1021/nn901648q.
50. Meyer, J.C.; Chuvilin, A.; Algara-Siller, G.; Biskupek, J.; Kaiser, U. Selective Sputtering and Atomic Resolution Imaging of Atomically Thin Boron Nitride Membranes. *Nano Lett.* **2009**, *9*, 2683–2689, doi:10.1021/nl9011497.
51. Li, X.; Hao, X.; Zhao, M.; Wu, Y.; Yang, J.; Tian, Y.; Qian, G. Exfoliation of Hexagonal Boron Nitride by Molten Hydroxides. *Adv. Mater.* **2013**, *25*, 2200–2204, doi:10.1002/adma.201204031.
52. Wang, X.; Zhi, C.; Li, L.; Zeng, H.; Li, C.; Mitome, M.; Golberg, D.; Bando, Y. "Chemical Blowing" of Thin-Walled Bubbles: High-Throughput Fabrication of Large-Area, Few-Layered BN and C x-BN Nanosheets. *Adv. Mater.* **2011**, *23*, 4072–4076, doi:10.1002/adma.201101788.
53. Wang, X. Bin; Weng, Q.; Wang, X.; Li, X.; Zhang, J.; Liu, F.; Jiang, X.F.; Guo, H.; Xu, N.; Golberg, D.; et al. Biomass-Directed Synthesis of 20 g High-Quality Boron Nitride Nanosheets for Thermoconductive Polymeric Composites. *ACS Nano* **2014**, *8*, 9081–9088, doi:10.1021/nn502486x.

54. Nag, A.; Raidongia, K.; Hembram, K.P.S.S.; Datta, R.; Waghmare, U. V.; Rao, C.N.R. Graphene Analogues of BN: Novel Synthesis and Properties. *ACS Nano* **2010**, *4*, 1539–1544, doi:10.1021/nn9018762.
55. Zhang, X., Qin, J., Xue, Y., Yu, P., Zhang, B., Wang, L., & Liu, R.. Effect of aspect ratio and surface defects on the photocatalytic activity of ZnO nanorods. Scientific reports, 4(1), 1-8. **2014**.
56. Gao, R.; Yin, L.; Wang, C.; Qi, Y.; Lun, N.; Zhang, L.; Liu, Y.X.; Kang, L.; Wang, X. High-Yield Synthesis of Boron Nitride Nanosheets with Strong Ultraviolet. *J. Phys. Chem. C* **2009**, *113*, 15160–15165, doi:10.1021/jp904246j.
57. Hasan, S.; Mamun, A.; Hussain, K.; Gaevski, M.; Ahmad, I.; Khan, A. Growth Evolution of High-Quality MOCVD Aluminum Nitride Using Nitrogen as Carrier Gas on the Sapphire Substrate. *J. Mater. Res.* **2021**, *36*, 4360–4369, doi:10.1557/S43578-021-00387-Z.
58. Hasan, S.; Mamun, A.; Hussain, K.; Patel, D.; Gaevski, M.; Ahmad, I.; Khan, A. Investigation of MOCVD Grown Crack-Free 4 Mm Thick Aluminum Nitride Using Nitrogen as a Carrier Gas. *MRS Adv.* **2021**, *6*, 456–460, doi:10.1557/S43580-021-00071-8.
59. Boo, J.H.; Rohr, C.; Ho, W. MOCVD of BN and GaN Thin Films on Silicon: New Attempt of GaN Growth with BN Buffer Layer. *J. Cryst. Growth* **1998**, *189–190*, 439–444, doi:10.1016/S0022-0248(98)00323-6.
60. Amano, H.; Kushimoto, M.; Nagamatsu, K.; Nitta, S.; Honda, Y.; Liu, Y.; Yang, X.; Pristovsek, M. Interface Amorphization in Hexagonal Boron Nitride Films on Sapphire Substrate Grown by Metalorganic Vapor Phase Epitaxy. *Appl. Phys. Express* **2018**, *11*, 051002, doi:10.7567/apex.11.051002.
61. Snure, M.; Paduano, Q.; Kiefer, A. Effect of Surface Nitridation on the Epitaxial Growth of Few-Layer Sp2BN. *J. Cryst. Growth* **2016**, *436*, 16–22, doi:10.1016/j.jcrysgro.2015.11.030.
62. Wu, Q.; Yan, J.; Zhang, L.; Chen, X.; Wei, T.; Li, Y.; Liu, Z.; Wei, X.; Zhang, Y.; Wang, J.; et al. Growth Mechanism of AlN on Hexagonal BN/Sapphire Substrate by Metal-Organic Chemical Vapor Deposition. *CrystEngComm* **2017**, *19*, 5849–5856, doi:10.1039/c7ce01064h.
63. Stadler, B.J.H. *Vapor Processes*; Elsevier Inc., **2016**; ISBN 9780123851321.
64. Tay, R.Y. *Chemical Vapor Deposition Growth and Characterization of Two-Dimensional Hexagonal Boron Nitride*; **2018**; ISBN 978-981-10-8808-7.
65. Nakamura, K.; Sasaki, T. Boron Nitride Films Prepared by MOCVD. *J. Solid State Chem.* **2000**, *154*, 101–106, doi:10.1006/jssc.2000.8818.
66. Han, M.; Ryu, B.D.; Ko, K.B.; Jo, C.H.; Lim, C. hyun; Cuong, T.V.; Han, N.; Hong, C.H. Characteristics of Aluminum Nitride Films on Hexagonal Boron Nitride Buffer Layers Using Various Growth Methods through Metal Organic Chemical Vapor Deposition. *J. Cryst. Growth* **2019**, *507*, 316–320, doi:10.1016/j.jcrysgro.2018.09.018.
67. Yang, F.H. *Modern Metal-Organic Chemical Vapor Deposition (MOCVD) Reactors and Growing Nitride-Based Materials*; Woodhead Publishing Limited, **2013**; ISBN 9780857095077.
68. Patriarche, G.; Ougazzaden, A.; Li, X.; Alam, S.; Sundaram, S.; Halfaya, Y. Wafer-Scale MOVPE Growth and Characterization of Highly Ordered h-BN on Patterned Sapphire Substrates. *J. Cryst. Growth* **2018**, *509*, 40–43, doi:10.1016/j.jcrysgro.2018.12.016.
69. Lee, H.-J.; Honda, Y.; Amano, H.; Bae, S.-Y.; Yang, X.; Pristovsek, M.; Nagamatsu, K.; Liu, Y.; Nitta, S. Growth of Hexagonal Boron Nitride on Sapphire Substrate by Pulsed-Mode Metalorganic Vapor Phase Epitaxy. *J. Cryst. Growth* **2017**, *482*, 1–8, doi:10.1016/j.jcrysgro.2017.10.036.
70. Eichler, J., & Lesniak, C.. Boron nitride (BN) and BN composites for high-temperature

applications. Journal of the European Ceramic Society, 28(5), 1105-1109. 2008.

71. McGregor, D.S.; Unruh, T.C.; McNeil, W.J. Thermal Neutron Detection with Pyrolytic Boron Nitride. *Nucl. Instruments Methods Phys. Res. Sect. A Accel. Spectrometers, Detect. Assoc. Equip.* **2008**, *591*, 530–533, doi:10.1016/j.nima.2008.03.002.

72. Caban, P.A.; Teklinska, D.; Michalowski, P.P.; Gaca, J.; Wojcik, M.; Grzonka, J.; Ciepielewski, P.; Mozdzonek, M.; Baranowski, J.M. The Role of Hydrogen in Carbon Incorporation and Surface Roughness of MOCVD-Grown Thin Boron Nitride. *J. Cryst. Growth* **2018**, *498*, 71–76, doi:10.1016/j.jcrysgro.2018.06.001.

73. Halfaya, Y.; Sundaram, S.; Patriarche, G.; Li, X.; Alam, S.; Salvestrini, J.P.; Voss, P.L.; Ougazzaden, A.; Ayari, T. MOVPE van Der Waals Epitaxial Growth of AlGaN/AlGaN Multiple Quantum Well Structures with Deep UV Emission on Large Scale 2D h-BN Buffered Sapphire Substrates. *J. Cryst. Growth* **2018**, *507*, 352–356, doi:10.1016/j.jcrysgro.2018.10.060.

74. Kobayashi, Y.; Akasaka, T. Hexagonal BN Epitaxial Growth on (0 0 0 1) Sapphire Substrate by MOVPE. *J. Cryst. Growth* **2008**, *310*, 5044–5047, doi:10.1016/j.jcrysgro.2008.07.010.

75. Jana, M.; Singh, R.N. Progress in CVD Synthesis of Layered Hexagonal Boron Nitride with Tunable Properties and Their Applications. *Int. Mater. Rev.* **2018**, *63*, 162–203, doi:10.1080/09506608.2017.1322833.

76. Maity, A.; Grenadier, S.J.; Li, J.; Lin, J.Y.; Jiang, H.X. Hexagonal Boron Nitride Neutron Detectors with High Detection Efficiencies. *J. Appl. Phys.* **2018**, *123*, doi:10.1063/1.5017979.

77. Han, M., Ryu, B. D., Ko, K. B., Jo, C. H., Lim, C. H., Cuong, T. V., & Hong, C. H.. Characteristics of aluminum nitride films on hexagonal boron nitride buffer layers using various growth methods through metal organic chemical vapor deposition. Journal of Crystal Growth, 507, 316-320, **2019**.

78. Yang, X., Nitta, S., Pristovsek, M., Liu, Y., Nagamatsu, K., Kushimoto, M., ... & Amano, H.. Interface amorphization in hexagonal boron nitride films on sapphire substrate grown by metalorganic vapor phase epitaxy. Applied Physics Express, 11(5), 051002, 2018.

79. Maity, A.; Doan, T.C.; Li, J.; Lin, J.Y.; Jiang, H.X. Realization of Highly Efficient Hexagonal Boron Nitride Neutron Detectors. *Appl. Phys. Lett.* **2016**, *109*, doi:10.1063/1.4960522.

80. Maity, A.; Grenadier, S.J.; Li, J.; Lin, J.Y.; Jiang, H.X. Toward Achieving Flexible and High Sensitivity Hexagonal Boron Nitride Neutron Detectors. *Appl. Phys. Lett.* **2017**, *111*, 1–5, doi:10.1063/1.4995399.

81. Ahmed, K.; Dahal, R.; Weltz, A.; Lu, J.J.Q.; Danon, Y.; Bhat, I.B. Solid-State Neutron Detectors Based on Thickness Scalable Hexagonal Boron Nitride. *Appl. Phys. Lett.* **2017**, *110*, 0–4, doi:10.1063/1.4973927.

82. Doan, T.C.; Marty, A.; Li, J.; Lin, J.Y.; Jiang, H.X. Thermal Neutron Detectors Based on Hexagonal Boron Nitride Epilayers. *Hard X-Ray, Gamma-Ray, Neutron Detect. Phys. XVIII* **2016**, *9968*, 99680S, doi:10.1117/12.2239079.

83. Doan, T.C.; Majety, S.; Grenadier, S.; Li, J.; Lin, J.Y.; Jiang, H.X. Hexagonal Boron Nitride Thin Film Thermal Neutron Detectors with High Energy Resolution of the Reaction Products. *Nucl. Instruments Methods Phys. Res. Sect. A Accel. Spectrometers, Detect. Assoc. Equip.* **2015**, *783*, 121–127, doi:10.1016/j.nima.2015.02.045.

84. Maity, A.; Grenadier, S.J.; Li, J.; Lin, J.Y.; Jiang, H.X. High Sensitivity Hexagonal Boron Nitride Lateral Neutron Detectors. *Appl. Phys. Lett.* **2019**, *114*, doi:10.1063/1.5098331.

85. Maity, A.; Grenadier, S.J.; Li, J.; Lin, J.Y.; Jiang, H.X. High Efficiency Hexagonal Boron Nitride Neutron Detectors with 1 Cm2 Detection Areas. *Appl. Phys. Lett.* **2020**, *116*,

doi:10.1063/1.5143808.

86. Murray, E.; Eden, M. (12 ) Patent Application Publication ( 10 ) Pub . No .: US 2005 / 0142206A1. **2005**, *1*, 1–4.
87. Moore, A.W.; Strong, S.L. (12) United States Patent. **2004**, *1*.
88. Du, X.Z.; Li, J.; Lin, J.Y.; Jiang, H.X. The Origin of Deep-Level Impurity Transitions in Hexagonal Boron Nitride. *Appl. Phys. Lett.* **2015**, *106*, doi:10.1063/1.4905908.
89. Doan, T.C.; Li, J.; Lin, J.Y.; Jiang, H.X. Bandgap and Exciton Binding Energies of Hexagonal Boron Nitride Probed by Photocurrent Excitation Spectroscopy. *Appl. Phys. Lett.* **2016**, *109*, doi:10.1063/1.4963128.
90. Spieler, H.G.; Haller, E. Assessment of Present and Future Large-Scale Semiconductor Detector Systems. *IEEE Trans. Nucl. Sci.* **1985**, *32*, 419–426, doi:10.1109/TNS.1985.4336867.
91. Many, A. High-Field Effects in Photoconducting Cadmium Sulphide. *J. Phys. Chem. Solids* **1965**, *26*, 575–578, doi:10.1016/0022-3697(65)90133-2.
92. Maity, A.; Grenadier, S.J.; Li, J.; Lin, J.Y.; Jiang, H.X. Effects of Surface Recombination on the Charge Collection in H-BN Neutron Detectors. *J. Appl. Phys.* **2019**, *125*, doi:10.1063/1.5089138.
93. Cao, X.K.; Clubine, B.; Edgar, J.H.; Lin, J.Y.; Jiang, H.X. Two-Dimensional Excitons in Three-Dimensional Hexagonal Boron Nitride. *Appl. Phys. Lett.* **2013**, *103*, doi:10.1063/1.4829026.
94. Nikolic, R.J.; Cheung, C.L.; Li; Reinhardt, C.E.; Wang, T.F. Roadmap for High Efficiency Solid-State Neutron Detectors. *spiedigitallibrary.org* **2005**, *15*, 601305, doi:10.1117/12.633256.
95. Clinton, J. Optimization and Characterization of a Novel Self Powered Solid State Neutron Detector. **2011**.
96. Doan, T.C.; Li, J.; Lin, J.Y.; Jiang, H.X. Response of Alpha Particles in Hexagonal Boron Nitride Neutron Detectors. *Appl. Phys. Lett.* **2017**, *110*, 1–6, doi:10.1063/1.4984112.
97. Dahal, R.; Ahmed, K.; Woei Wu, J.; Weltz, A.; Jian-Qiang Lu, J.; Danon, Y.; Bhat, I.B. Anisotropic Charge Carrier Transport in Free-Standing Hexagonal Boron Nitride Thin Films. *iopscience.iop.org* **2016**, *9*, doi:10.7567/APEX.9.065801.